Mem. S.A.It. Suppl. Vol. 11, 220

Memorie della
Supplementi

Planetary soil simulation:

binary mixtures reflectance spectra

S. Montanaro, R. Politi, A. Blanco, A. Dinoi, S. Fonti, A.C. Marra, G.A. Marzo, and V. Orofino

Università degli Studi di Lecce, Dipartimento di Fisica, C.P. 193, 73100 Lecce,
tel: +39 0832 297550, fax: +39 0832 297505, e-mail: sarah.montanaro@le.infn.it

Abstract. Inhomogeneities of a planetary surface imply the necessity of an accurate study of the mixing laws of intimate mixtures. This work is aimed to obtaining a deconvolution procedure of surface spectra necessary to interpret the main features of planetary surface spectra, such as composition and particle size. Our method is based on the use of laboratory intimate mixtures of materials of Martian interest. Such mixtures are analysed by means of Hapke theory that in turn can be used to simulate synthetic spectra of different mixtures which can be then experimentally tested.

1. Introduction

Looking at the surface of a planet with remote sensing techniques we are obviously recording a spectrum of a mixture of different minerals with different grain size. Therefore in order to determine the mineralogy of the observed surface it is necessary to apply a deconvolution procedure. In this work we try to define a deconvolution procedure based on a mixed approach, both theoretical and experimental. In fact we apply Hapke theory (Hapke, 1981; Hapke & Wells, 1981) to laboratory spectra of mixtures, trying to obtain information about the mass and the granulometry of components. The measurements are performed in hemispherical reflectance in the Visible-Near-Infra-Red (VNIR: 0.7 ÷ 2.5 μm) and Medium-Infra-Red (MIR: 2.5 ÷ 25 μm) ranges. We chose to use the hemispherical reflectance because it can be easily applied, by means of Kirchhoff's law, even in the range of thermal-infra-red where emission is dominant. In addition, it is quite simple to be performed in laboratory since reflectance spectra do not depend on the observational geometry. In fact, even if the measurement obtained by remote sensing are bi-directional, the information about orientation of grain is lost because of the distance between surface and detector, and therefore it could be reduced to hemispherical reflectance laboratory measurements. On the other hand the grain orientation is dominant in laboratory measurements performed with a bi-directional configuration. In this work we present a first application of this deconvolution technique to mixtures of materials of Martian interest such as sulphates (gypsum, $CaSO_4 * 2H_2O$) (Arvidson et al., 2006) and carbonates (dolomite, $CaMg(CO_3)_2$) (Bandfield et al., 2003; Lellouch et al., 2000). The grain size of both minerals has been chosen according to the typical Martian surface grain size, between

Send offprint requests to: S. Montanaro

$100 \div 200\ \mu m$ (Dollfus et al., 1993; Edgett & Christensen, 1994).

2. Theoretical approach

The Hapke reflectance theory (Hapke, 1981) for intimate mixtures has been already tested by Johnson et al. (1983) and Clark (1983) for the VNIR region, but, since the current techniques of remote sensing can investigate longer wavelenghts, it is important testing this theory also in MIR region. Assuming spherical particles with isotropic scattering, the directional-hemispherical reflectance, r_h could be described by equations

$$r_h = \frac{1}{\mu_0} \int_{2\pi} r(i, e, g) \mu d\Omega_e \tag{1}$$

$$\begin{aligned} r(i, e, g) \; = \; & \frac{w}{4} \frac{\mu_0}{\mu + \mu_0} \{[1 + B(g)]p(g) + \\ & + H(\mu_0)H(\mu) - 1\}. \end{aligned} \tag{2}$$

where μ_0 is the cosine of the zenith angle of incidence i, μ is the cosine of the zenith angle of emergence e, $r(i, e, g)$ is the bi-directional reflectance, w is the single-scattering albedo, $B(x)$ the opposition effect function, $p(g)$ the volume angular-scattering function, $H_(x)$ the Chandrasekar function and g is the phase angle.

Developing $p(g)$ with Legendre Polynomials at the second order, we obtain

$$\begin{aligned} r_h \; = \; & \frac{1 - \gamma}{1 + 2\mu_0\gamma} + \frac{w}{4} \frac{\mu_0}{1 + 2\mu_0} \xi \cdot \\ & \cdot \left[\frac{5}{4} \xi (3\mu_0^2 - 1) - 3 \right] \end{aligned} \tag{3}$$

Due to the large number of particles present in the observed samples and to the random orientation of the grains, we can assume the cosine asymmetry factor, ξ, equal to zero. Under this hypothesis, the reflectance becomes:

$$r_h = \frac{1 - \gamma}{1 + 2\mu_0\gamma} \tag{4}$$

with

$$\gamma = \sqrt{1 - w} \tag{5}$$

and

$$w = \frac{Q_S}{Q_E} \tag{6}$$

where Q_S is the scattering efficiency and Q_E the extinction efficiency.

The intimate mixture consists of different particles mixed homogeneously together in close proximity, like in planetary regoliths. In this case the reflectance is:

$$r_m = \frac{1 - \gamma_m}{1 + 2\mu_0\gamma_m} \tag{7}$$

with

$$\gamma_m = \sqrt{1 - w_m} \tag{8}$$

and

$$w_m = \frac{\sum_j N_j \sigma_j Q_S}{\sum_j N_j \sigma_j Q_E} = \frac{\sum_j \frac{M_j Q_{S_j}}{\rho_j D_j}}{\sum_j \frac{M_j Q_{E_j}}{\rho_j D_j}} \tag{9}$$

where, for jth spices, N_j is the number of particles per unit volume, ρ_j the solid density, σ_j the geometrical cross-sectional area, M_j the bulk density and D_j the equivalent size.

3. Measurements

The main characteristics of the minerals we used are listed in table 1 while the actual size distribution is shown in figure 1. We have examined mixtures with different mass percentages of each component, but in this paper we focus only on the mixture at 50% in weight ($2.8092 \pm 0.0001\ g$ of gypsum and $2.8028 \pm 0.0001\ g$ of dolomite).

Table 1. Characteristics of the mineral samples used for mixtures.

mineral	density (g/cm^3)	size (μm)
gypsum	2.30	169.10
dolomite	2.84	133.89

In figure 2 (VNIR) and 3 (MIR) the reflectance of the each separate component is shown.

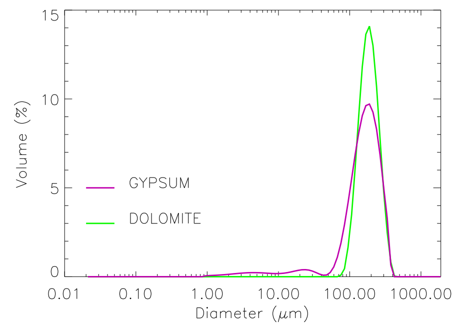

Fig. 1. Measured grain size distribution for the gypsum and the dolomite samples, discussed in the text.

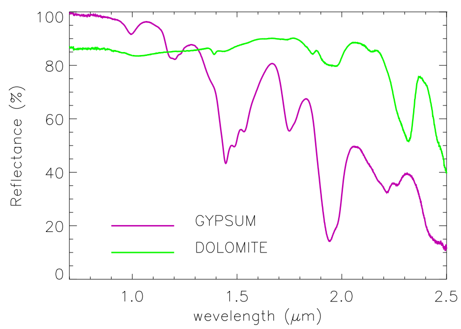

Fig. 2. Reflectance spectra of gypsum and dolomite in VNIR region.

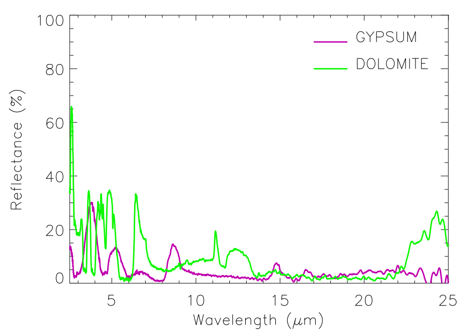

Fig. 3. Reflectance spectra of gypsum and dolomite in MIR region.

In figure 4 and 5 we show the measured and calculated reflectance of the mixture.

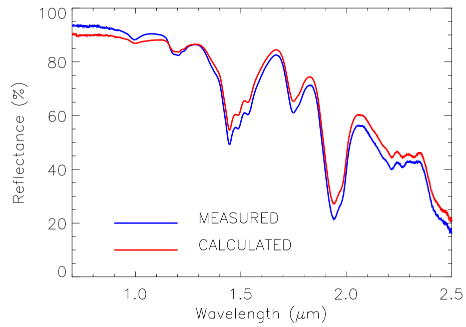

Fig. 4. Measured and calculated reflectance spectra of a mixture 50% gypsum and 50% dolomite in VNIR region.

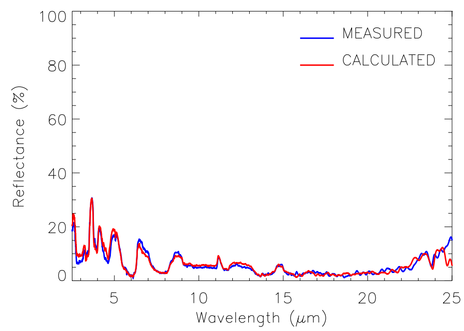

Fig. 5. Measured and calculated reflectance spectra of a mixture 50% gypsum and 50% dolomite in MIR region.

The agreement between the two spectra, theoretical and experimental, is quite good, but in the MIR region there are some small differences especially in the resstrahlen bands. Such effect could be much larger as we can be seen in figure 6 which is relative to another mixture of calcite ($CaCO_3$) (Bandfield et al., 2003) and quartz (SiO_2) (Bandfield et al., 2004; Bandfield, 2006).

The reason of such discrepancies is due to the assumption $Q_E = 1$, because it is not valid in correspondence of the resstrahlen bands, where $Q_A \gg Q_S$, and so the normalization $Q_E = Q_A + Q_S = 1$ cannot be used any longer. It is therefore necessary to consider separately Q_S and Q_E instead of their ratio w. However, in this case, we cannot use anymore a single two

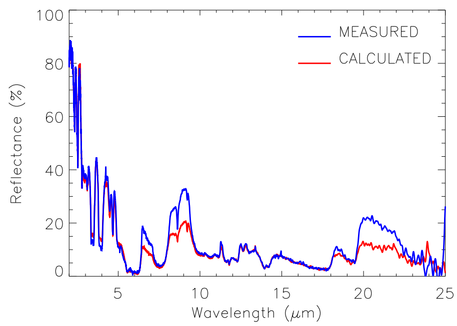

Fig. 6. Measured and calculated reflectance spectra of a mixture 50% calcite and 50% quartz in MIR region.

components mixtures, since, under this new hypothesis, the number of variables is larger then the number of the equations. We thought to bypass the problem using another material and producing other two binary mixtures that, together with the measured spectrum of the third material, would allow to write a system of six equations with six variables. We chose olivine ($(Fe, Mg)SiO_4$) (Bibring et al., 2006) as third material of planetary interest.

$$\begin{cases} w_g = \frac{Q_{S_g}}{Q_{E_g}} \\ w_d = \frac{Q_{S_d}}{Q_{E_d}} \\ w_{ol} = \frac{Q_{S_{ol}}}{Q_{E_{ol}}} \\ w_{g+d} = \frac{\frac{M_g}{\rho_g D_g} Q_{E_g} w_g + \frac{M_d}{\rho_d D_d} Q_{E_d} w_d}{\frac{M_g}{\rho_g D_g} Q_{E_g} + \frac{M_d}{\rho_d D_d} Q_{E_d}} \\ w_{g+ol} = \frac{\frac{M_g}{\rho_g D_g} Q_{E_g} w_g + \frac{M_{ol}}{\rho_{ol} D_{ol}} Q_{E_{ol}} w_{ol}}{\frac{M_g}{\rho_g D_g} Q_{E_g} + \frac{M_{ol}}{\rho_{ol} D_{ol}} Q_{E_{ol}}} \\ w_{d+ol} = \frac{\frac{M_d}{\rho_d D_d} Q_{E_d} w_d + \frac{M_{ol}}{\rho_{ol} D_{ol}} Q_{E_{ol}} w_{ol}}{\frac{M_d}{\rho_d D_d} Q_{E_d} + \frac{M_{ol}}{\rho_{ol} D_{ol}} Q_{E_{ol}}} \end{cases} \quad (10)$$

Unfortunately the above system has ∞^3 solutions and therefore cannot be of any help. For this reason we decide to turn back to equations (4) and (7) and use for one of the variables an independently measured value. For this purpose we performed a transmittance measurement of the dolomite sample from which we are able to derive the value of Q_{E_d} (shown in figure 7), by means of following equation:

$$\frac{Q_{E_d}}{a} = \frac{4}{3}\frac{\rho S}{M} \ln \frac{1}{T(\lambda)} \quad (11)$$

where a is the radius of particle, $S = \pi r^2$ with r the pellet radius, M is the mass of dolomite and ρ its density.

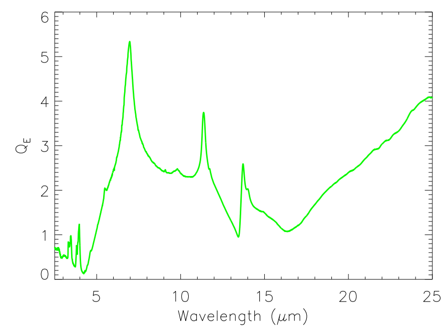

Fig. 7. Dolomite extiction efficiencies evaluated from transmittance measurements.

In order to verify the applicability of this procedure, we measured also the absorption efficiency, Q_{A_d}, by means of a transmission measurement performed on the same sample of dolomite placed at the entrance of an integrating sphere. The result of the measurement has been compared with the value of Q_{A_d} obtained using the Hapke reflectance theory. The result is shown in figure 8 and there are some important differences between the two spectra. The main discrepancies are related to the level of the continuum and to the inversion of the resstrahlen bands (around 7 μm and beyond 22 μm) in the measured spectra. The latter effect is probably due to the lack of saturation of such bands in the transmittance measurements, while the same bands are certainly fully saturated in reflectance. In spite of the detected discrepancies, we have tried to derive by means the reflectance theory the value of extinction efficiency of gypsum, Q_{E_g}, with the purpose to check the feasibility of the method presented in

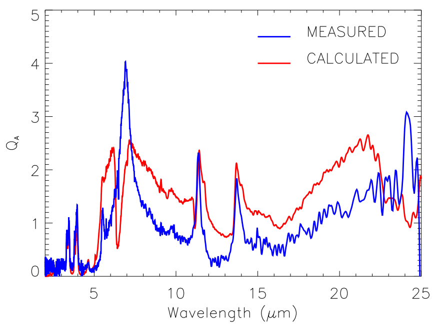

Fig. 8. Measured and calculated dolomite absorption efficiency.

this paper. As it can be seen in figure 9, the results seem encouraging and we plan to go on in this work using only reflectance measurements.

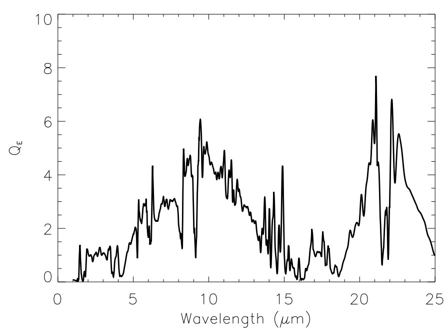

Fig. 9. Calculated extinction efficiency of gypsum.

4. Conclusions

The work presented here is only at a preliminary stage, but we think it is interesting to illustrate the complexity of the subject and the difficulties of comparing laboratory and planetary spectra. We have checked that the use at the same time of transmittance and reflectance measurements poses serious problem to the interpretation of the results. Therefore the next step will be to use both hemispherical and bi-directional reflectance measurements and check that the obtained results are consistent with each other. The final validation of the procedure described in this paper will allow a more accurate interpretation of planetary surface spectra taken with remote sensing techniques.

References

Arvidson, R. E., Squyres, S. W., Anderson, R. C., et al. 2006, Journal of Geophysical Research (Planets), 111, 2

Bandfield, J. L. 2006, Geophys. Res. Lett., 33, 6203

Bandfield, J. L., Glotch, T. D., & Christensen, P. R. 2003, Science, 301, 1084

Bandfield, J. L., Hamilton, V. E., Christensen, P. R., & McSween, H. Y. 2004, Journal of Geophysical Research (Planets), 109, 10009

Bibring, J.-P., Langevin, Y., Mustard, J. F., et al. 2006, Science, 312, 400

Clark, R. N. 1983, J. Geophys. Res., 88, 10635

Dollfus, A., Deschamps, M., & Zimbelman, J. R. 1993, J. Geophys. Res., 98, 3413

Edgett, K. S. & Christensen, P. R. 1994, J. Geophys. Res., 99, 1997

Hapke, B. 1981, J. Geophys. Res., 86, 3039

Hapke, B. & Wells, E. 1981, J. Geophys. Res., 86, 3055

Johnson, P. E., Smith, M. O., Taylor-George, S., & Adams, J. B. 1983, J. Geophys. Res., 88, 3557

Lellouch, E., Encrenaz, T., de Graauw, T., et al. 2000, Planet. Space Sci., 48, 1393